simplifications made in the derivation of this formula seem to be well justified (§ 5.19). From the function $P_0^{(\pi)}(E_0,E)$ one can obtain the other track lengths with simple operations (§ 5.16). As E approaches zero, P_0 approaches the value P_0/ϵ_0, p_0 diverges logarithmically, and g_0 diverges as $1/E$ (§ 5.18). As E approaches E_0, $P_0^{(\pi)}$ and $P_0^{(\gamma)}$ go to zero, $p_0^{(\pi)}$ goes to $1/\epsilon_0$, $p_0^{(\gamma)}$ goes to zero, $g_0^{(\pi)}$ goes to zero, and $g_0^{(\gamma)}$ behaves as a δ-function (§ 5.18).

Computations of the track lengths with the correct cross-sections for the elementary processes are available. The computations of Rossi and Klapman give $P_0^{(\pi)}(E_0,E)$ and $P_0^{(\gamma)}(E_0,E)$ for one fixed value of $E(E = 10^7$ ev) as functions of E_0. The computations of Richards and Nordheim give the various track lengths for $E_0 \gg \epsilon_0$, as functions of E (§ 5.20). The results of these computations do not differ much from those of Tamm and Belenky.

CHAPTER

6

Experimental Results on the Electromagnetic Interactions of High-Energy Particles in Cosmic Rays and from Artificial Sources

6.1. ***Introduction.*** The interactions between elementary particles and matter fall into two categories, depending on whether the forces that come into play are mainly electromagnetic or mainly nuclear in character. The results of the theory of electromagnetic interactions have been described in Chapters 2 and 5. A satisfactory theory of nuclear interactions is still wanting, even though many nuclear phenomena can be explained on the basis of a few comparatively simple assumptions.

In the present and in the following chapters there are collected some experimental results that can be used to check the theory of electromagnetic interactions and to obtain information on nuclear interactions of high-energy particles. The experiments to be described were made partly with rays from terrestrial sources (radioactive substances, high-energy accelerators) and partly with cosmic rays. The radiation from a terrestrial source has usually a known composition and often consists of particles all of a given type and of a given energy. Cosmic rays, on the contrary, contain particles of many different kinds with a wide energy distribution whose shape is *a priori* unknown.

Cosmic-ray experiments have the twofold purpose of determining the composition of the radiation and providing information on the interactions with matter of the various particles contained in it. In many cases the two problems cannot be separated, but must be solved simultaneously. This represents a peculiar difficulty of cosmic-ray research. One is confronted with it whenever one tries to interpret cosmic-ray experiments and again whenever one attempts to describe the results of these experiments in a logical sequence. Thus, we shall be led occasionally

into discussing the composition of cosmic rays, even though this subject does not logically belong in the present volume.

In selecting the material for this and the subsequent chapters, we have chosen to consider as "high-energy particles" particles with energies greater than the binding energies of nucleons in nuclei; i.e., greater than about 10 Mev. Also we have placed greater emphasis on experimental results bearing on the properties of elementary particles than on experimental results bearing on the structure of atoms and nuclei.

6.2. *Electromagnetic interactions of high-energy photons.* Some of the theoretical conclusions presented in Chapter 2 on the interactions of high-energy photons with matter were tested by artificially produced γ-rays.

Delsasso, Fowler, and Lauritsen (DLA37) measured the absorption of γ-rays produced by bombardment of a Li^7 target with artificially accelerated protons. The interactions of protons with Li^7 nuclei gives rise to excited Be^8 nuclei. In their transitions to the ground state, these nuclei emit a main group of γ-rays of 17.5-Mev energy and a weaker group of about 14-Mev energy.

As a detector, Delsasso and his collaborators used a cloud chamber placed in a magnetic field and divided into two halves by a 0.032-cm-thick lead plate. They observed the electron pairs produced by materialization of the photons in the plate. By selecting pairs whose total energy corresponded to 17.5 Mev, within the experimental errors, they were able to rule out the low-energy group of γ-rays completely.

The experiment consisted of determining the rate of production of electron pairs in the lead plate both with and without a 1-cm-thick lead absorber between the source and the cloud chamber. Monitoring of the γ-ray beam made it possible to correct for any change in the source intensity during the experiment and thus to compute the attenuation of photons in the lead absorber.

Note that, because of the criterion used for the selection of pairs, the detector was not sensitive to γ-rays of energy appreciably smaller than that of the incident rays. Therefore it had a very small likelihood of recording γ-rays that had undergone Compton scattering in the absorber, for in most Compton collisions the secondary electron carries away a large fraction of the energy of the incident photon (§ 2.18). Likewise it could not record the strongly degraded γ-rays arising from radiation processes of the electrons produced by materialization of the photons in lead. Thus the observed attenuation measured the probability for the photons to undergo either Compton scattering or materialization in traversing the lead plate.

From the value of this attenuation the total absorption coefficient corresponding to these two phenomena was found to be 0.058 ± 0.006 cm^2 g^{-1}. On the other hand, the theoretical values of the absorption coefficients of 17.5-Mev γ-rays for Compton effect and for pair production are 0.008 and 0.057 cm^2 g^{-1} respectively. Thus the experimental absorption coefficient appeared to be somewhat smaller than the total theoretical absorption coefficient (0.065 cm^2 g^{-1}) even though the difference was hardly outside the experimental errors.

Gamma rays of energy higher than that of γ-rays from nuclear reactions can be obtained by means of *betatrons* or *synchrotrons*. These machines produce mono-energetic beams of electrons, which, upon striking a target, give rise to secondary γ-rays distributed continuously in energy from zero to the energy E of the electrons themselves. If the target is very thin, so that the electrons do not lose any appreciable energy before radiating the quanta, the differential energy spectrum of γ-rays (number of photons per unit energy interval) is represented, apart from a proportionality constant, by the same function that represents the differential radiation probability (§ 2.11). If the electron energy, E, is sufficiently large this function is roughly proportional to $1/E'$, where E' is the energy of the secondary photon. Thus, the thin target spectrum of a betatron or a synchrotron radiation has the following approximate expression:

$$\gamma(E') = \text{const}/E' \qquad \text{for } E' < E,$$
$$\gamma(E') = 0 \qquad \text{for } E' > E. \tag{1}$$

One can compute more accurate expressions for $\gamma(E')$ by using the correct formulae for the radiation probability and by taking into account the finite thickness of the target (SLI46; PWM51). For example, the heavy curve in Fig. 1 shows the theoretical spectrum of the γ-ray beam from a synchrotron operated at 330 Mev with a 0.05-cm thick platinum target. The thin line shows the corresponding spectrum for an infinitely thin target. The γ-ray spectrum of the same synchrotron was determined experimentally from cloud-chamber observations of pairs produced in a 0.0025 cm lead foil (PWM51). The experimental data were in good agreement with the theoretical predictions (this result, incidentally, may be regarded as a direct check of the radiation theory).

Experiments on γ-rays obtained by means of the 100-Mev General Electric betatron were reported by Lawson (LJL49). From the betatron beam Lawson selected γ-rays in a narrow range of energies (88 ± 1 Mev) by means of a pair-production detector. Figure 2 represents schematically the experimental arrangement. The γ-radiation from the source passes through a hole in a lead screen, through the absorber, through a collimator, and then falls onto a thin pair-forming target. The collimator consists essentially of a lead box with two opposite holes, in which a strong magnetic field is maintained. This collimator removes secondary electrons generated in the absorber by the γ-ray beam and it also helps in preventing scattered γ-rays from reaching the target. The electron pairs formed in

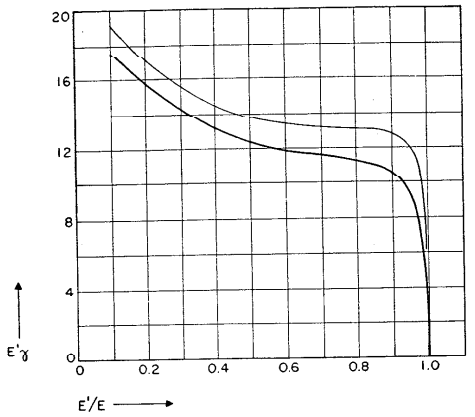

Fig. 6.2.1. The thin line represents the γ-ray spectrum produced by 330-Mev electrons striking an infinitely thin platinum target. The heavy line represents the γ-ray spectrum produced by the same electrons striking a 0.05 cm thick platinum target. The abscissa, E'/E, is the ratio of the photon energy to the electron energy. The ordinate, $E'\gamma(E')$, is the number of γ-rays per unit energy interval multiplied by the γ-ray energy. The data were taken from a paper by Powell *et al.* (PWM51).

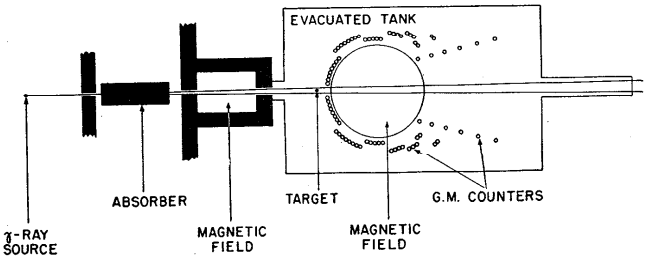

Fig. 6.2.2. Experimental arrangement used by Lawson for measuring γ ray absorption (LJL49).

the target are bent by a magnetic field and are then detected by an array of Geiger-Mueller counters. An elaborate coincidence circuit selects coincidences between pairs of such counters so arranged as to respond only to electron pairs whose total energy is 88 ± 1 Mev.

The results of absorption measurements in various elements are shown in Fig. 3, which gives the ratio of the theoretical to the experimental absorption coefficients as a function of the square of the atomic number Z. These experiments, like those of Delsasso and his collaborators described above, indicate that the absorption coefficient of γ-rays in heavy elements is appreciably smaller than that obtained from the theory. In light elements, with the possible exception of beryllium, the difference between the experimental and the theoretical absorption coefficients is not significantly greater than the experimental error.

Similar results were obtained by Adams (AGD48), who measured the absorption coefficient in aluminum, iron, and copper of γ-rays of 11, 14, and 19 Mev from a betatron source. Similar results were also obtained by Walker (WRL49.1; WRL49.2), who measured very accurately both the total absorption coefficient and the probability of pair production in various elements for 17.5-Mev photons from the proton-lithium reaction. Note, however, that Walker's measurements with lithium and carbon did not confirm the small discrepancy between experimental and theoretical absorption coefficients in substances of low atomic numbers suggested by Lawson's measurement with beryllium (see Fig. 3).

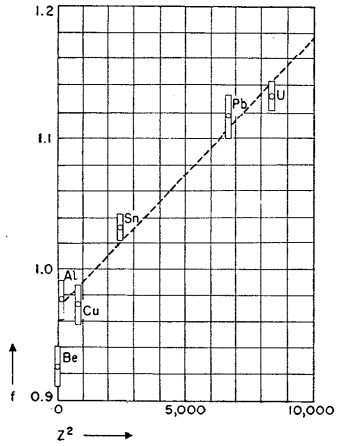

Fig. 6.2.3. Ratio, f, of the theoretical to the experimental absorption coefficient of 88-Mev γ-rays, as a function of the square of the atomic number of the absorber. The theoretical absorption coefficient is the sum of the absorption coefficients for Compton effect and for pair production. The absorption coefficient for pair production is obtained from the theory of Wheeler and Lamb (WJA39), which includes pair production in the field of electrons. From Lawson (LJL49).

In elements of high atomic numbers, pair production is predominant. Therefore the experimental results described above point to the existence of an error in the computation of the probability for pair production. Very likely, this error does not imply any failure of the fundamental principles of the theory, but reflects merely the inadequacy of the mathematical approximation (Born approximation) used in obtaining the numerical results. As already pointed out in § 2.11, one may expect from this approximation an error proportional to Z^2. The experimental results are consistent with this conclusion; moreover, they indicate that in the energy interval

explored, which extends from 10 Mev to 88 Mev, the relative error is approximately independent of energy, and amounts to about 12 per cent for lead.

6.3. *Photo-disintegrations.* High-energy photons are capable of disrupting nuclei, a phenomenon known as the *photo-disintegration.* This phenomenon, even though it affects the nuclear structure, is here included in the category of electromagnetic interaction because it may be looked upon as the effect of an electromagnetic field on the charges and on the magnetic moments of the elementary particles that form the nuclei.

Photo-disintegration leads very often to the formation of β-active isotopes, whose nature can easily be recognized by the characteristic mean life. Therefore the most common procedure for the detection of photo-disintegrations consists of irradiating the sample and subsequently investigating its β-activity by means of a Geiger-Mueller counter. Photo-disintegrations leading to the emission of charged particles have also been observed by means of cloud chambers and photographic emulsions. Photo-disintegrations leading to the emission of neutrons have been detected by means of BF_3 counters and by the neutron activation of rhodium foils.

In all elements and for all energies the number of γ-rays that produce photo-disintegrations is a small fraction of those that undergo Compton effect or materialization. Therefore one cannot use an absorption measurement to determine the cross-section for a photo-disintegration process. In order to obtain this cross-section one must measure the absolute number of photo-disintegrations produced by a known number of γ-rays traversing a given sample. The cross-section, σ, is then given by the following equation:

$$\text{number of disintegrations per } \gamma\text{-ray} = \frac{N}{A} x\sigma, \tag{1}$$

where N is the number of atoms per gram-atom, A the atomic mass number, and x the thickness of the sample in g cm^{-2}. Such absolute determinations offer very great difficulties and therefore the experimental data on the absolute cross-section of nuclei for photo-disintegrations are still scarce and inaccurate.

Experiments on photo-disintegrations have been made with monoenergetic photons from nuclear reactions and with the continuous γ-ray spectrum obtained by means of betatrons or synchrotrons. Among the measurements of the first kind, one may quote those of Waffler and Hirzel (WfH48) who determined quantitatively the (γ,n) cross-section of Cu^{63} for 17.5-Mev γ-rays obtained by bombardment of lithium with protons. For this cross-section they found a value of $(1.6 \pm 0.4) \cdot 10^{-25}$ cm^2. The same authors also measured the (γ,n) and (γ,p) cross-sections of many other elements relative to the (γ,n) cross-section of Cu^{63} (WfH47).

Betatron and synchrotron sources afford the possibility of measuring the variation with photon energy of the cross-sections for photo-disintegrations. One can perform this measurement by varying the energy, E, of the electron beam and measuring the specific activity of the sample as a function of this energy. As pointed out in § 0.2, the γ-rays produced by a betatron are distributed continuously in energy from zero to a maximum equal to the energy of the electrons. Thus the number, $n(E)$, of photo-disintegrations produced by the γ-ray beam of a betatron operated at an energy E is represented by the equation:

$$n(E) = k \int_0^E \sigma(E')\gamma(E,E')\, dE', \tag{2}$$

where k is a constant, $\sigma(E')$ is the cross-section for photo-disintegration by photons of energy E', and the function $\gamma(E,E')$ represents the differential spectrum of the γ-radiation produced by electrons of energy E. We assume here that the sample is thin so that one may neglect the number of photons undergoing Compton effect or pair production.

If one uses the approximate expression for the function $\gamma(E,E')$ given by Eqs. (6.2.1), the integrand in Eq. (2) becomes independent of E and differentiation with respect to E yields:

$$\sigma(E) = \text{const } E \frac{dn}{dE}. \tag{3}$$

Equation (6.2.1) represents only a crude approximation and it is thus necessary to use a relation more elaborate than Eq. (3) in order to obtain the best estimate for the variation of σ with photon energy from the observed variation of n with electron energy. Even so, the results are not as accurate as those that one could obtain if mono-energetic γ-ray sources of variable energy were available.

The most common type of photo-disintegration is a (γ,n) reaction; i.e., the emission of a single neutron from the nucleus. However, other types of reactions are also possible, such as (γ,p) and (γ,α) reactions, multiple disintegrations and photo-fissions. In a light nucleus, the (γ,p) or (γ,α) reaction may occur at energies lower than the minimum energy for the production of the (γ,n) reaction. For example, C^{13} irradiated with γ-rays of more than about 7.6-Mev energy disintegrates into three α-particles, whereas the threshold for the (γ,n) reaction in C^{12} is 18.6 Mev.

Multiple disintegrations, i.e., disintegrations in which more than one particle is emitted from the nucleus, occur in many and possibly all elements when the photon energy is sufficiently high. For example, Baldwin and Klaiber (BGC48) have published the picture of a 4-prong "star" produced in the gas of a cloud chamber by the γ-ray beam of a betatron operated at 100 Mev. This star corresponds presumably to the following reaction:

$$_7N^{14} + \gamma \rightarrow {}_1H^1 + 3\ {}_2He^4 + {}_0n^1.$$

Photo-fission is known to take place in Th^{232}, U^{233}, U^{235}, U^{238}, and Pu^{239}.

For each nucleus and for each type of photo-disintegration there exists a well-defined threshold energy. Table 1 lists some representative results of threshold measurements made by different experimenters with betatron

Table 6.3.1. Thresholds for some photo-disintegrations. The theoretical values were computed from known nuclear masses [see also refs. (OWE50.1) and (OWE50.2)]

Reaction	Observed Threshold Energy (Mev)	Computed Threshold Energy (Mev)	Reference
$H^2(\gamma,n)H^1$	2.20 ± 0.05	2.19 ± 0.03	(MEJ49)
$C^{12}(\gamma,n)C^{11}$	18.7 to 19.4	18.7 ± 0.3	(BGC45)
$N^{14}(\gamma,n)N^{13}$	10.65 ± 0.2	10.51 ± 0.1	(MEJ49)
$O^{16}(\gamma,n)O^{15}$	16.3 ± 0.4	15.6 ± 0.6	(BGC45)
$Mg^{24}(\gamma,n)Mg^{23}$	16.2 ± 0.3	15.5 ± 1.0	(MEJ49)
$Al^{27}(\gamma,n)Al^{26}$	14.0 ± 0.4	11.1 ± 1.0	(MEJ49)
$Si^{28}(\gamma,n)Si^{27}$	16.8 ± 0.4	16.0 ± 1.0	(MEJ49)
$P^{31}(\gamma,n)P^{30}$	12.35 ± 0.2	11.1 ± 1.0	(MEJ49)
$S^{32}(\gamma,n)S^{31}$	14.8 ± 0.4	16.7 ± 0.5	(MEJ49)
$K^{39}(\gamma,n)K^{38}$	13.2 ± 0.4	12.7 ± 1.5	(MEJ49)
$Ca^{40}(\gamma,n)Ca^{39}$	15.9 ± 0.4	13.7 ± 1.5	(MEJ49)
$Fe^{54}(\gamma,n)Fe^{53}$	13.8 ± 0.2		(MEJ49)
$Cu^{63}(\gamma,n)Cu^{62}$	10.9 + 0.2		(MEJ50)
$Cu^{65}(\gamma,n)Cu^{64}$	10.2 ± 0.2		(MEJ49)
$Ag^{109}(\gamma,n)Ag^{108}$	9.3 ± 0.5		(BGC45)
$Sb^{121}(\gamma,n)Sb^{120}$	9.25 ± 0.2		(MEJ49)
$Au^{197}(\gamma,n)Au^{196}$	8.00 ± 0.15		(HAO49)
$Hg^{201}(\gamma,n)Hg^{200}$	6.25 ± 0.20		(HAO49)
$Pb^{206}(\gamma,n)Pb^{205}$	8.25 ± 0.10		(PH50)
$Pb^{207}(\gamma,n)Pb^{206}$	6.95 ± 0.10		(PH50)
$Pb^{208}(\gamma,n)Pb^{207}$	7.44 ± 0.10		(PH50)
$Bi^{209}(\gamma,n)Bi^{208}$	7.45 ± 0.2		(MEJ49)
$Li^7(\gamma,p)He^6$	9.8 ± 0.5	10.1 ± 0.5	(MEJ49)
$Mg^{25}(\gamma,p)Na^{24}$	11.5 ± 1.0	10.9 ± 1.0	(MEJ49)
$Mg^{26}(\gamma,p)Na^{25}$	14.0 ± 1.0	15.0 ± 1.6	(MEJ49)
$Th^{232}(\gamma,\text{fission})$	5.40 ± 0.22		(KHW50)
$U^{233}(\gamma,\text{fission})$	5.18 ± 0.27		(KHW50)
$U^{235}(\gamma,\text{fission})$	5.31 ± 0.25		(KHW50)
$U^{238}(\gamma,\text{fission})$	5.08 ± 0.15		(KHW50)
$Pu^{239}(\gamma,\text{fission})$	5.31 ± 0.27		(KHW50)

sources. It appears that, whenever a comparison has been made, the observed threshold energy is close to the minimum energy required by the reaction, as computed from known nuclear masses.

It should be emphasized that the photo-disintegrations investigated so far are not necessarily among those with largest cross-sections. In fact,

most experimenters detected photo-disintegrations by observing the activity of the residual nuclei. This method selects photo-disintegrations leading to nuclei with easily detectable activities, i.e., to fairly short-lived radio-active isotopes.

As the photon energy is increased beyond the threshold, the cross-section increases rapidly at first, goes through a fairly sharp maximum, and then decreases rapidly again. This behavior of the excitation curves for photo-disintegrations was first demonstrated by Baldwin and Klaiber

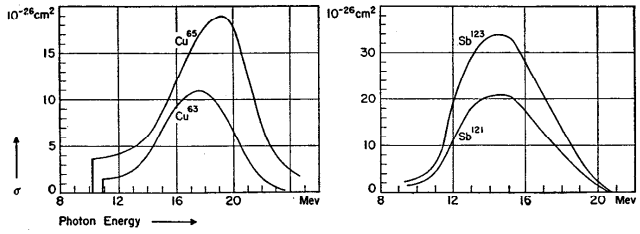

Fig. 6.3.1. Cross-sections for the (γ,n) reactions of Cu^{63}, Cu^{65}, Sb^{121}, Sb^{123}, as measured by Johns, Katz, Douglas, and Haslam (JHE50).

(BGC48). Quantitative data on the variation of the cross-section with energy are available only for some of the (γ,n) reactions. Figure 1 represents the results obtained by Johns, Katz, Douglas, and Haslam (JHE50) on the (γ,n) reactions of Cu^{63}, Cu^{65}, Sb^{121}, and Sb^{123}. For other results on the same subject the reader may consult refs. (BGC48), (MEJ49), and (DBC50).

Table 6.3.2. The threshold energy, E_T, the energy at the maximum, E_m, the maximum cross-section, σ_m; the width at half-maximum of the excitation curve, ΔE; and the integrated cross-section, $\int_0^\infty \sigma(E)\,dE$, for various photo-disintegrations. [From Johns *et al.* (JHE50).]

Reaction	E_T Mev	E_m Mev	σ_m 10^{-24} cm²	ΔE Mev	$\int\sigma(E)\,dE$ Mev · 10^{-24} cm²
$Cu^{63}(\gamma,n)Cu^{62}$	10.9	17.5	0.11	6.0	0.70
$Cu^{65}(\gamma,n)Cu^{64}$	10.2	19.0	0.18	6.0	1.40
$Sb^{121}(\gamma,n)Sb^{120}$	9.3	14.5	0.21	5.5	1.2
$Sb^{123}(\gamma,n)Sb^{122}$	9.3	14.5	0.34	5.5	2.0
$Ta^{181}(\gamma,n)Ta^{180}$	8.0	13.5	0.078	4.5	0.39

A quantity of interest is the integrated cross-section, defined as

$$\int_0^\infty \sigma(E)\, dE.$$

Table 2 summarizes the experimental determinations of this quantity for several (γ,n) reactions. The same table also indicates the threshold energy, the position of the maximum, the maximum value of the cross-section, and the width at half-maximum of the excitation curve.

One may mention that, according to some theoretical arguments (GM48; LJS50) the integrated cross-section of a nucleus of mass number A should approximately equal $0.02A$ 10^{-24} cm^2 Mev. The cross-section considered here includes all kinds of disintegrations that may occur after the nucleus has been brought into an excited state by the absorption of a photon.

6.4. ***Momentum loss of charged particles in matter.*** Most of the available experimental evidence regarding momentum losses of high-energy particles in matter comes from cloud-chamber observations on cosmic-ray particles. In these experiments one usually places the absorbing plate across the cloud chamber so as to divide it into two halves, and measures the curvature of the tracks going through the plate both in the upper and in the lower half of the chamber. The presence of the plate considerably increases the difficulty of eliminating spurious distortions, and makes it necessary to adopt special precautions to obtain reliable results [see, for instance, (BPM37)]. In order to avoid this difficulty and to use thicker absorbers, some experimenters have employed two separate cloud chambers, with the absorbing plate placed between them (EP38).

For particle velocities at which the accuracy of the measurements is limited by distortion rather than by scattering, the mean error in the determination of a momentum p is p^2/p_0, where p_0 is the maximum detectable momentum (see § 3.13). On the assumption that the momentum loss is small compared with the initial momentum of the particle, the relative error in the measurement of a momentum loss, Δp, by a particle of momentum p is $\sqrt{2}\, p^2/(p_0 \Delta p)$. When collision losses predominate, Δp is approximately independent of p (§ 2.5). When radiation losses predominate, Δp is approximately proportional to p (§ 2.11). In either case one sees that the accuracy of the measurements of momentum losses decreases rapidly with increasing momentum.

It is hardly necessary to point out that, unless appropriate precautions are taken, the use of counter control (§ 3.10) may greatly distort the results of experiments intended to determine the average momentum loss of a group of particles or the relative probability of various momentum losses. For example, if the chamber is triggered by two counters, of which one is above and the other below the chamber, no particle that stops in the plate will be detected. Also, particles that come out of the plate with small energy may not be able to reach the lower counter because of the strong deflection of their trajectories in the magnetic field and because of the large mean angle of scattering. In this case, therefore, counter control discriminates against large momentum losses.

In §§ 4.3 and 4.6 we have already described those experiments on the momentum loss of cosmic-ray particles that led to the identification of the positive electron and of the meson. In this section we shall describe briefly some other experiments that supplied quantitative data on the momentum losses of high-energy electrons and of heavier particles.

Anderson and Neddermeyer (NSH35; ACD36) operated a magnet chamber containing a 0.35-cm-thick lead plate both at Pasadena (sea level) and at Pike's Peak (4,200 meters altitude). They triggered the cloud chamber with the coincident pulses of two Geiger-Mueller counters, one above, the other below the chamber. However, in the measurements of momentum losses they disregarded those particles that were responsible for the coincidences between the two Geiger-Mueller counters and took into consideration only particles traversing the cloud chamber simultaneously with the triggering particles. Most of the particles thus selected were *electrons*, as electrons often occur in showers whereas practically all mesons and protons occur singly. Moreover, the method of selection removed the instrumental discrimination against particles undergoing large momentum losses.

Table 1 shows the average momentum losses measured by Neddermeyer and Anderson for particles in different momentum groups, along with the corresponding theoretical values for the average momentum losses of electrons. The agreement between experiment and theory is far from perfect, but is as good as one could expect, considering the small numbers of tracks measured and the large errors of the individual measurements. One may regard this result as a crude check of the theoretical formula for the radiation loss of electrons, or, alternately, as an experimental proof that shower particles are indeed electrons.

In § 2.13 we have pointed out that the theory predicts large fluctuations in the radiation losses. According to theory, the probability of a high energy electron losing, by radiation, a given fraction of its momentum in a given absorber is approximately independent of the initial momentum. It is thus possible to compare the observed fluctuations with the theoretical predictions by grouping the observed particles according to *fractional* momentum losses. This was done by Blackett (BPM38). Figures 1 and 2 show the results of his measurements with lead plates of 0.33-cm and 1.0-cm thickness respectively, along with the corresponding theoretical curves. The relative momentum loss plotted as abscissa is the quantity:

$$R = \frac{2[p_1 - p_2 - (\Delta p)_{\text{col}}]}{(p_1 + p_2)d}, \tag{1}$$

Table 6.4.1. Average momentum losses per cm of lead of cosmic-ray electrons as a function of the momentum. (Except where otherwise indicated the theoretical momentum losses are computed at the two ends of the momentum interval specified at the head of the column. Sea level measurements; field 4,500 gauss; absorber 0.35 cm of lead.) [Anderson and Neddermeyer (ACD36).]

Momentum Interval in Mev/c	<50	50–100	100–150	150–200
Number of tracks	22	28	15	16
Momentum loss in Mev/c per cm of Pb:				
observed	37	81	124	207
theoretical radiation	36*	77–160	160–250	250–330
theoretical collision	14*	15–16	16–17	17–18
theoretical total	50*	92–176	176–267	267–348

* Computed at 26 Mev/c.

Measurements at 4,100 meters; field 7,900 gauss; absorber 0.35 cm of lead. [Anderson and Neddermeyer (ACD36).]

Momentum Interval (Mev/c)	<50	50–100	100–150	150–200	200–400
Number of tracks	29	65	18	13	21
Momentum loss in Mev/c per cm of Pb:					
observed	42	82	178	191	358
theoretical radiation	38*	77–160	160–250	250–330	330–680
theoretical collision	14*	15–16	16–17	17–18	18–20
theoretical total	52*	90–177	177–260	260–350	350–700

* Computed at 31 Mev/c.

where p_1 and p_2 are the momenta of the electron above and below the lead plate respectively, $(\Delta p)_{col}$ is the computed momentum loss by collision, and d is the thickness of the plate in centimeters. The theoretical curves are computed from Eq. (2.13.2). The agreement between theory and experiment is satisfactory, considering the approximations of the theory and the experimental uncertainties.

Ehrenfest (EP38) and Wilson (WJG38; WJG39) reported the results of measurements performed at sea level on the momentum loss of cosmic-ray particles in fairly large thicknesses of matter. As an absorber, Ehrenfest used a 9-cm-thick lead block placed between two cloud chambers, Wilson used a 2-cm-thick gold block placed across a cloud chamber. Both Ehrenfest and Wilson selected particles that traversed the absorber without producing showers or other secondary effects. This selection effec-

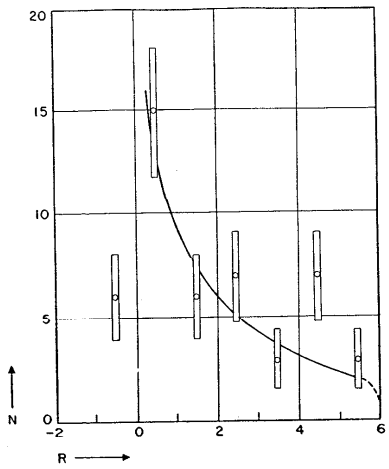

Fig. 6.4.1. Distribution of momentum loss of cosmic-ray electrons in a 0.33-cm lead plate, from cloud-chamber experiments. B = 3,300 gauss. Initial momentum $<2.10^8$ ev/c. The abscissa represents the relative momentum loss, R, defined by Eq. (1). The ordinate represents the observed number of particles, N, per unit interval of R. From Blackett (BPM38).

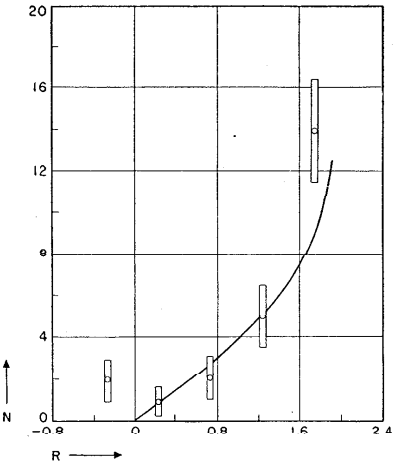

Fig. 6.4.2. Distribution of momentum loss of cosmic-ray electrons in a 1-cm lead plate. Initial momentum $<2.10^8$ ev/c. From Blackett (BPM38).

tively rules out all electrons. Thus the results obtained refer either to *mesons* or to *protons*.

Table 6.4.2. Momentum losses of cosmic-ray particles of non-electronic nature near sea level. (The two values of the theoretical momentum loss listed refer to the two extremes of the momentum interval.)

Author	Momentum Range (10^8 ev/c)	Number of Particles Investigated	Momentum Loss in 10^6 ev/c per cm Gold		
			Experimental	Theoretical (μ-mesons)	Theoretical (protons)
Ehrenfest (EP38)	2–10	24	28	22–25	1500–30
Wilson (WJG39)	2–4	19	20.7 ± 3.5	22–22	1500–100
Wilson (WJG39)	4–7	30	24.5 ± 6.2	22–24	100–50

Table 2 summarizes the experimental data on the average momentum loss of particles in different momentum intervals, along with the theoretical values for the collision losses of μ-mesons and protons, computed at the two extremes of each interval (see § 2.9; in this computation the collision loss per g cm^{-2} of gold was taken as equal to that of lead). The measurements considered in Table 2 cover a range of momenta extending from $2 \cdot 10^8$ to 10^9 ev/c. In this range the observed average momentum losses agree with the theoretical momentum losses of μ-mesons (note that for mesons as well as for protons below 10^9 ev/c, radiation losses are negligible compared with collision losses). The measurements are accurate enough to rule out the possibility that, at sea level, more than a small fraction of cosmic-ray particles with momenta between $2 \cdot 10^8$ and 10^9 ev/c may have protonic mass. They are not, however, accurate enough to distinguish between π- and μ-mesons.

6.5. ***Scattering of cosmic-ray particles in matter.*** Measurements on the tracks of charged particles in photographic emulsions have furnished the most accurate experimental test of the theory of multiple Coulomb scattering available to date. In § 3.15 we already have dealt with these measurements briefly. In this section we wish to describe some earlier cloud-chamber experiments on the scattering of cosmic-ray particles. These experiments provided the first rough check of the theory of Coulomb scattering for high-energy particles and are still important on account of their bearing on the problem of nuclear scattering.

The experimental arrangements used for cloud-chamber experiments on scattering are essentially identical to those used in the measurements of momentum losses except that the requirements in the accuracy of the momentum determinations are much less stringent. Indeed, in some cases, momentum measurements have been omitted altogether even though knowledge of the momenta of the individual particles is very desirable,

especially on account of the strong energy dependence of the probability for Coulomb scattering (see §§ 2.15, 2.16, and 2.17).

The experimental investigation of scattering of high-energy electrons is closely related to the study of showers. Here we shall restrict our discussion to the behavior of the heavier, non-radiating particles in cosmic rays. According to the conclusions reached previously (see §§ 4.11 and 6.4) most charged cosmic-ray particles near sea level are either electrons or μ-mesons. Thus the experiments to be described mainly yield information on the electromagnetic and nuclear scattering of these particles.

Strictly speaking, one should not consider nuclear scattering separately from other nuclear interactions. The change in direction of a high-energy particle colliding against a nucleus must often be accompanied by a disruption of the nucleus. If some of the disintegration products emerge from the plate where the collision occurs, the phenomenon will be described as a nuclear disintegration; otherwise, as a scattering process. For this reason we shall postpone until Chapter 8 the discussion of those data on nuclear scattering that fit naturally into the general discussion of nuclear interactions. Here we shall limit ourselves to a description of experiments on the angular distribution of scattered particles and to a discussion of the information on nuclear scattering arising from discrepancies between the observed distributions and those computed from the theory of Coulomb scattering.

Usually the quantity measured is not the total angle of scattering, but its projection on a plane perpendicular to the axis of the chamber. Under the limitations discussed in § 2.16, the theory of Coulomb scattering gives the following expression for the root mean square value, θ_m, of the projected angle of scattering [see Eqs. (2.16.7) and (2.16.10)]:

$$\theta_m = \langle \theta^2 \rangle_{\text{av}}^{1/2} = \frac{E_s}{\sqrt{2}\,\beta c p}\, t^{1/2}, \tag{1}$$

where $E_s = 21$ Mev, t is the thickness of material traversed in radiation lengths, p is the momentum, and βc the velocity of the particle.

Equation (1) can be rewritten as follows:

$$\langle \beta^2 c^2 p^2 \theta^2 \rangle_{\text{av}}^{1/2} = \frac{E_s}{\sqrt{2}}\, t^{1/2}. \tag{2}$$

This equation shows that one can test experimentally the theory of multiple scattering by computing the average value of the product $\beta^2 c^2 p^2 \theta^2$ for particles of different momenta traversing a given plate. Wilson analyzed in this manner some experimental data obtained at sea level by Blackett and himself on penetrating particles with momenta between $2 \cdot 10^8$ and $2 \cdot 10^9$ ev/c (BPM38; WJG40) and found satisfactory agreement with the theoretical predictions.

A similar result was reported by Code (CFL41) who measured scattering angles and momenta of 359 particles ($p < 2 \cdot 10^9$ ev/c) traversing 3.8 cm of wolfram (72.5 g cm^{-2}). From his measurements, Code computed the arithmetic mean of $|\beta cp\theta|$ and found the value $|\beta cp\theta|_{av} = 2.14 \cdot 10^9$ ev degrees. For 3.8 cm of wolfram the theoretical value of $\langle\beta^2c^2p^2\theta^2\rangle_{av}^{1/2}$ is $2.8 \cdot 10^9$ ev degrees; under the assumption of a Gaussian distribution, the corresponding value of $|\beta cp\theta|_{av}$ is $\sqrt{2/\pi} \cdot 2.8 \cdot 10^9 = 2.2 \cdot 10^9$ ev degrees, in good agreement with the experimental result.

For a discussion of the experimental results on the distribution of scattering angles we recall that, when multiple scattering predominates, this distribution is theoretically represented by a Gaussian function (see § 2.17). With the value of θ_m given by Eq. (1), we may write the distribution function as follows:

$$Q\left(\frac{\theta}{\theta_m}\right) d\left(\frac{\theta}{\theta_m}\right) = \frac{d\theta}{\sqrt{2\pi}\,\theta_m} \exp\left(-\frac{\theta^2}{2\theta_m{}^2}\right). \tag{3}$$

Since θ_m is inversely proportional to pc, one sees that the distribution function is independent of momentum if one uses the product $pc\theta$ as an independent variable, whereas with the ratio θ/θ_m as an independent variable, the distribution function becomes independent of momentum *and* thickness. Thus it is again possible, for the purpose of analysis, to group data concerning mesons of different momenta and also data obtained with different scattering plates, provided the condition for multiple scattering, Eq. (2.17.14), is satisfied in all cases.

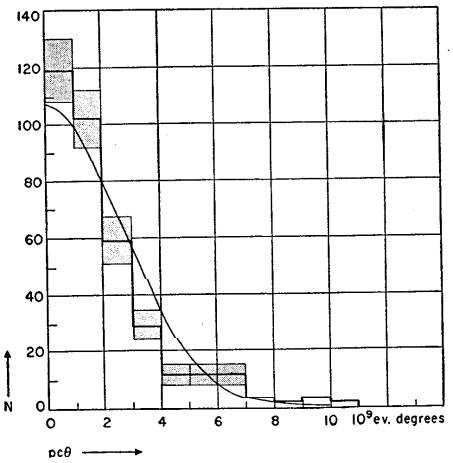

Fig. 6.5.1. The distribution of cosmic-ray particles scattered by 3.8 cm of wolfram, plotted against the product $pc\theta$; θ is the projected angle, and p the momentum. The histogram represents the observed distribution and the corresponding statistical errors. The curve is the theoretical gaussian curve computed for μ-mesons. From Code (CFL41).

Wilson analyzed his data by plotting the distribution of scattering events observed with different plates as a function of θ/θ_m. Code did a similar analysis of the data obtained with 3.8 cm of wolfram by using $pc\theta$ as a variable. The condition for multiple scattering was well satisfied in Code's experiments; not, however, in all of Wilson's experiments. Both Wilson and Code found that their experimental points could be fitted satisfactorily to the theoretical Gaussian curve. As an example, Fig. 1 shows the results of Code's analysis. Thus there seems to be general agreement between theory and experiment on the subject of scattering of high-energy particles.

However, Wilson as well as Code reported the observation of a few events in which the angle of scattering was greater than the maximum angle that one would reasonably expect to observe as a result of Coulomb interaction. Wilson found one event of this kind in the group of experiments summarized in Table 1, in which the total thickness of matter traversed was approximately equivalent to 4 meters of lead. He found another similar event in a group of photographs representing a total scattering layer of about 50 meters of lead, but unsuitable for accurate momentum measurements. In this event, the deflection of the incident particle was accompanied by the ejection of a low-energy proton from the plate, a clear indication of nuclear interaction.

Code reported the observation of 10 tracks for which the value of $\beta cp\theta$ was greater than $8 \cdot 10^9$ ev degrees on a total of 450 traversals of 3.8 cm of wolfram. The Gaussian distribution predicts only 1.5 events of this kind. On the other hand, it is difficult to explain these events as examples of single Coulomb scattering, for the finite size of the wolfram nucleus causes the probability of this process to go rapidly to zero for values of the product $pc\theta$ greater than about $1.4 \cdot 10^9$ ev degree [see Eq. (2.15.14)]. It thus seems likely that the majority of the observed large-angle scattering processes represent nuclear interactions.

Further results on scattering of penetrating cosmic-ray particles have been reported by Vargus (VJA39), by Shutt (SRP42.1; SRP46), and by Sinha (SMS45). Vargus did not find any significant deviation from the theoretical predictions. Both Shutt and Sinha detected some discrepancies when they compared with one another the distributions of scattering angles obtained with different thicknesses of the scattering plate. Note that neither Shutt nor Sinha measured the momenta of individual particles,

even though Sinha, by means of an anti-coincidence arrangement, selected particles within given intervals of range.

Despite the results of the two last authors, if one takes the experimental evidence as a whole, one feels justified in stating the following conclusions. (a) The small-angle scattering of penetrating particles observed at sea level does not differ appreciably from the theoretical Coulomb scattering of mesons. (b) There are, however, a few instances of large-angle scattering that are difficult to explain as electromagnetic interactions and are probably due to nuclear encounters. According to the meager experimental data, the mean free path for these interactions may be as small as several meters of lead or as large as several tens of meters of lead.

Conclusion (a) confirms the fact that most of the penetrating particles at sea level are mesons. Protons, in the momentum ranges considered by both Wilson and Code, have velocities appreciably less than the velocity of light and are therefore more strongly scattered than mesons by Coulomb interaction alone. Scattering experiments, however, do not rule out the possibility that some of the penetrating particles observed near sea level are protons. Indeed it may be possible to explain most or all of the rare instances of anomalous scattering as nuclear scattering of protons. It is interesting to note, in this connection, that only one of the strongly scattered particles in Code's experiments is listed as negative, whereas six are positive and the remaining are of undetermined sign.

6.6. ***The discovery of showers.*** In 1932 Rossi (RB32.2) placed three Geiger-Mueller counters in a "triangular" arrangement (see Fig. 1)

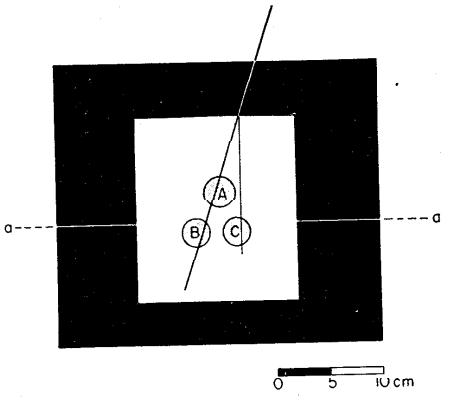

Fig. 6.6.1. Experimental arrangement used by Rossi for the detection of showers by means of coincidences between Geiger-Mueller tubes (RB32.2).

so that they could not be simultaneously discharged by a single ionizing particle traveling on a straight line. With the counters surrounded by lead, as shown in the figure, he recorded 35.5 ± 1 coincidences per hour. After removing the upper part of the lead shield (above the plane a-a) he found that the counting rate dropped to 10.0 ± 0.5 per hour. Rossi interpreted these results as evidence for the production of secondary ionizing particles by cosmic rays in lead.

The coincidences observed without lead were still in excess of the expected rate of chance coincidences (see § 3.7). About one-third of them were shown to arise from secondary particles scattered back by the lower part of the shield; the residual effect was tentatively ascribed partly to chance coincidences and partly to secondary effects occurring in the counter walls and in the lead on the sides of the counters [see (RB33.1); secondary effects from the air and from the ceiling or the walls of the laboratory may have played a role too].

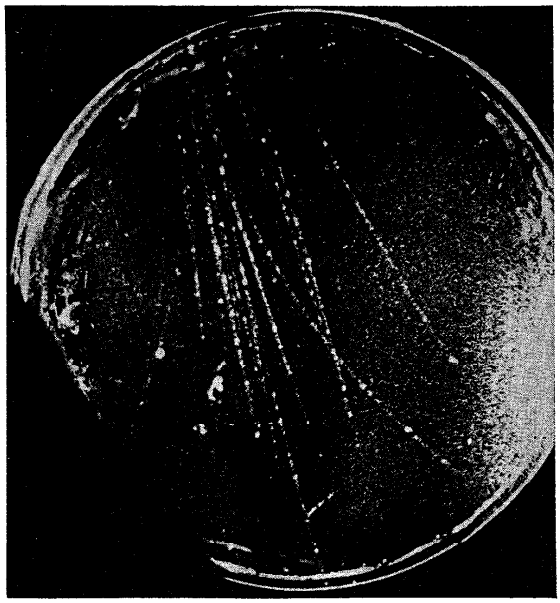

Fig. 6.6.2. One of the early pictures of cascade showers obtained by Blackett and Occhialini in a magnetic field of 3,100 gauss. The shower originates from the copper coils. The tracks curved to the left belong to negative electrons; the tracks curved to the right belong to positive electrons (BPM33).

This experiment marked the beginning of extensive experimental work on the secondary effects of cosmic rays. The next important development came in 1933 when Blackett and Occhialini (BPM33) began a systematic investigation of cosmic-ray phenomena by means of counter-controlled cloud chambers (see § 3.10). The cloud chamber used in their first experiments was operated in a magnetic field of several thousand gauss and was controlled by the coincident discharges of two Geiger-Mueller counters placed one above and the other below the chamber. In many of the photographs thus obtained Blackett and Occhialini found groups of apparently associated tracks. Some of these pictures showed that occasionally cosmic rays give rise to secondary events of astounding complexity, which the authors called *showers* (see Fig. 2).

Shower particles seemed to be, at least for the most part, positive and negative electrons with energies between 10^7 and 10^8 ev. They generally appeared to diverge downwards from some region in the material surrounding the chamber. Sometimes they seemed to originate from a single point or a small volume, while in other cases two or more radiating points could be detected. In some experiments, Blackett and Occhialini placed a 0.4-cm-thick lead plate across the chamber. With this arrangement they found that when a shower enters the chamber from above, often a new shower started in the plate. In some cases the secondary shower appeared to be produced by a "non-ionizing link."

Physicists thought, at first, that cosmic-ray showers were the result of some peculiar type of interaction between high-energy particles and atomic nuclei. This interpretation met immediately with one serious difficulty. Indeed, one might have expected to find mainly protons and heavier nuclear fragments among the products of nuclear interactions. The experiments of Blackett and Occhialini instead had shown that shower particles are mainly electrons.

The possibility of "explosive" elementary processes, whereby many electrons are produced simultaneously, was investigated theoretically by Heisenberg (HsW36). In the meantime, however, the rapidly increasing experimental information on the properties of showers on the one hand, and the quantitative development of quantum electro-dynamics on the other suggested an entirely different interpretation of cosmic-ray showers. In fact it became apparent that one could explain the complex features of showers under the assumption that showers are the result of radiation processes by electrons and pair production by photons. The theory of this phenomenon has been discussed in detail in Chapter 5.

It is known today that both nuclear interactions and electron-photon cascade processes occur in cosmic rays. Most of the showers observed near sea level, however, are due to processes of the latter type.

In the following sections we shall describe a few among the many experiments on cosmic-ray showers that served to establish the character

of this phenomenon and provided a check of the shower theory. For more detailed information on this subject we refer the reader to a review article by Froman and Stearns (FDK38).

6.7. *Geiger-Mueller experiments on showers.* Rossi used "triangular" arrangements of Geiger-Mueller counters of the type shown in Fig. 6.6.1 to investigate the rate of occurrence of showers under layers of different thickness and of different materials (RB33.1; RB33.3). The results obtained with lead are represented in Fig. 1. The curve shown

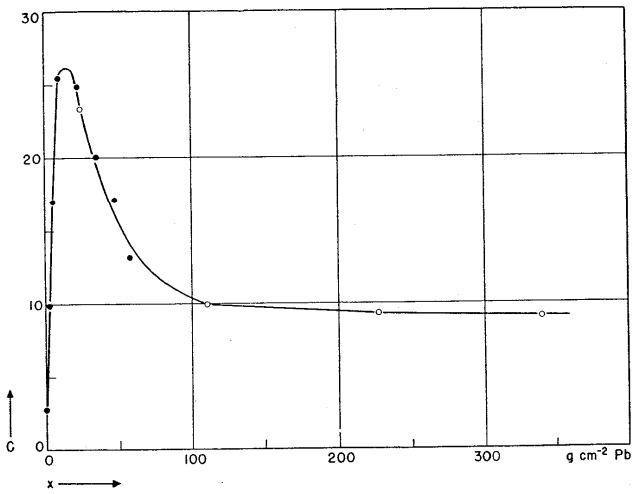

Fig. 6.7.1. The transition curve for showers in lead obtained with "triangular" arrangements of Geiger-Mueller tubes, of the type shown in Fig. 6.6.1. The abscissa represents the thickness, x, of the lead above the counter. The ordinate represents the counting rate, C. The solid dots and the open circles refer to two different measurements, made with slightly different geometrical arrangements. The corresponding counting rates are normalized to the same value at around 24 g cm^{-2} (RB33.1; RB33.3).

in this figure rises rapidly to a maximum at about 20 g cm^{-2} of lead, falls off again beyond the maximum, rapidly at first but then more and more slowly, until, beyond a thickness of about 100 g cm^{-2}, it becomes almost parallel to the horizontal axis.

Rossi interpreted the characteristic shape of the shower curve in lead by assuming that the observed showers were initiated by two different agents: a "soft radiation," which is very effective in producing showers

and, for this reason, is rapidly absorbed, and a "hard radiation," which is less effective in producing showers and can therefore penetrate large thicknesses of lead without appreciable absorption. According to this view the "soft rays" are responsible for the sharp maximum at about 20 g cm^{-2} and the "hard rays" for the "tail" of the shower curve.

The above interpretation still holds, if one but renames the soft rays "electrons and photons" and the hard rays "μ-mesons."

Electrons and photons incident upon lead from the atmosphere multiply into showers that reach their maximum development for a lead thickness of several radiation lengths and are then rapidly absorbed. Therefore if only electrons and photons were present, the shower curve would fall rapidly to zero beyond the maximum.

However, in addition to electrons and photons, cosmic rays near sea level contain a large number of μ-mesons. While most μ-mesons traverse the absorber without producing any conspicuous secondary effect, some give rise to high-energy electrons or photons by electromagnetic interactions (collision processes, radiation processes, pair production). Each secondary electron or photon will then multiply into a shower capable of discharging the triangular array of counters. The coincidence rate due to showers initiated by mesons increases rapidly at first with increasing lead thickness, goes through a flat maximum at a lead thickness corresponding to the average "range" of the showers, and then decreases slowly, following the absorption curve of μ-mesons.

High-energy protons and neutrons also are capable of producing coincidences in a shower-detecting arrangement under lead by virtue of their nuclear interactions (see § 8.2). However, near sea level, these particles are very rare compared to μ-mesons and for this reason their effects are relatively unimportant. This is no longer true at high elevation, where the number of nucleons relative to that of μ-mesons is greater than at sea level.

For a quantitative discussion of the shower curves one should take into account: (a) the energy distribution of electrons and photons incident upon the absorber or generated in the absorber by mesons; (b) the probability for each of these electrons or photons to produce a shower of N particles in the given absorber; (c) the probability that a shower of N particles emerging from the absorber gives rise to a coincidence with the particular array of counters used. None of these quantities can be readily determined. Therefore an accurate comparison with theory of the experimental shower curves represents a very difficult task, and one that has never been accomplished satisfactorily despite several attempts.* One can show, however, that there is at least an approximate agreement between experiment and theory.

* See, for example, N. Arley, *On the Theory of Stochastic Processes and Their Application to the Theory of Cosmic Rays*, Gads Forlag, Copenhagen (1948). See also (AN38; AN40).

According to the theory, the average number of particles in a shower initiated by an electron or photon of energy E_0 has a maximum at a thickness of the order of $\ln (E_0/\epsilon_0)$ where ϵ_0 is the critical energy (see §§ 5.13 and 5.22). Since the probability of a coincidence increases with increasing number of shower particles, electrons or photons of energy E_0 will produce the maximum number of coincidences under about $\ln (E_0/\epsilon_0)$ radiation lengths.

Cosmic-ray electrons and photons are not mono-energetic; the number of these particles per unit energy interval decreases rapidly with increasing energy and therefore most of the observed coincidences will be produced by electrons and photons with energy not much greater than the minimum energy necessary to produce a shower of the required size. This size depends on the experimental arrangement used for the detection of showers. If we assume, for instance, that the average shower recorded in Rossi's experiment contains from 2 to 6 particles, the average value of E_0/ϵ_0 is between 20 and 70 (see Fig. 5.22.2). The corresponding position of the maximum is between 5 and 6 radiation lengths (see Fig. 5.22.1), in approximate agreement with the curve shown in Fig. 1.

The arguments presented above lead one to predict that the thickness at which the maximum of the shower curve occurs depends on the experimental arrangement and increases with the number of shower particles that are necessary to produce the required coincidence. Comparison between the shower curves obtained with different numbers and dispositions of counters confirms this conclusion (FDK38).

The dependence of shower production on atomic number of the producing layer was first investigated by Rossi. Figure 2 compares the results obtained with producing layers of lead and iron, placed in the same position relative to the counters. In this figure, the abscissa represents the thickness of the producing layer in g cm^{-2}. One sees that the shower curve for iron goes through its maximum at a larger thickness than the shower curve for lead and that the iron maximum is lower than the lead maximum.

Both of these results are in qualitative agreement with the prediction of the shower theory.

As for the magnitude of the maximum, note that, according to theory, the number of particles at the optimum thickness is approximately proportional to E_0/ϵ_0. Therefore the minimum energy of electrons or photons capable of producing a shower of the required size is greater in the case of iron, for which $\epsilon_0 = 21$ Mev, than in the case of lead, for which $\epsilon_0 = 7.6$ Mev (see Table 5.24.1). The effective number of shower-producing particles is correspondingly smaller in the first than in the second case.

As for the position of the maximum, consider that the average size of showers recorded is determined mainly by the experimental arrangement and is thus approximately the same at the lead maximum as at the iron maximum. This means that in both cases the effective value of E_0/ϵ_0 for electrons and photons capable of producing coincidences is approximately

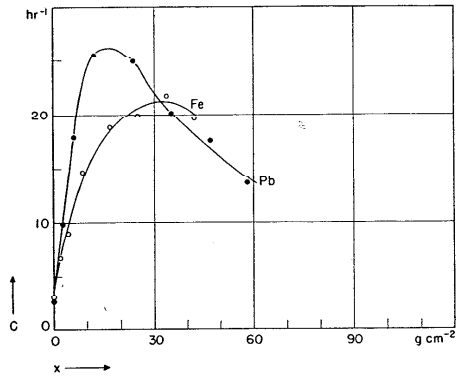

Fig. 6.7.2. Transition curves for showers in lead and iron, obtained with a "triangular" arrangement of Geiger-Mueller counters (RB33.1).

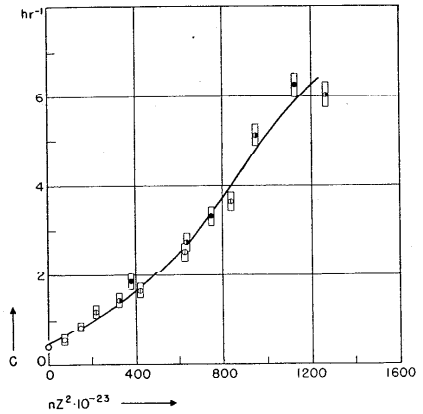

Fig. 6.7.3. The initial parts of the transition curves for showers in lead ●, tin ◑, zinc ⊖, and aluminum ○, plotted against nZ^2 (n: number of atoms per cm³; Z: atomic number). From Hu Chien Shan (HCS37).

the same. Thus the optimum thickness is roughly the same in iron and lead when measured in radiation lengths. When measured in g cm^{-2}, it is roughly proportional to the radiation length, which is greater in iron (14 g cm^{-2}) than in lead (6.5 g cm^{-2}; see Table 5.24.1).

When the thickness of the shower-producing layer is small compared with the thickness where the shower curve reaches its maximum, collision losses of electrons should not play an important role in the development of showers, and different materials should behave in a similar manner with regard to shower production provided their thickness is measured in radiation lengths. That this conclusion is correct is shown by the experimental results of HuChien Shan (HCS37) summarized in Fig. 3. In this figure the counting rates recorded under various thicknesses of different substances are plotted against the product nZ^2 where $n = xN/A$ represents the number of atoms per cm² of the producing layer and Z is the atomic number. Thus the abscissa in Fig. 3 is approximately proportional to the thickness in radiation lengths. One sees that the experimental points obtained with different elements lie close to a single smooth line, as expected.

6.8. ***Shower production by photons. Absorption coefficients of cosmic-ray photons.*** Figure 1 represents the experimental arrangement used by Janossy and Rossi (JL40.1) to investigate showers produced by cosmic-ray photons separately from showers produced by electrons and mesons. The two counters D were connected in parallel and so were

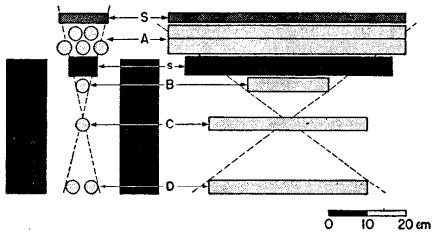

Fig. 6.8.1. Experimental arrangement used by Janossy and Rossi for the investigation of shower production by cosmic ray-photons (JL40.1).

the five counters A. The counter tray A covered the whole solid angle subtended by counters B,C,D. Threefold coincidences (BCD) and fourfold coincidences ($ABCD$) were recorded simultaneously. The difference between their numbers gives the number of coincidences (BCD) that are not accompanied by discharges of counters A [anti-coincidences ($BCD - A$)].

Anti-coincidences cannot be produced by ionizing particles coming from above because these particles cannot traverse counters B,C, and D without traversing A. Photons, however, traverse counters A undetected. When some material is present between A and B, they can produce in this material electron pairs or more complex showers that discharge counters B,C,D, and thus give rise to anti-coincidences. Therefore, the curve that

represents the rate of anti-coincidences as a function of the thickness of the materials between A and B may be regarded as the transition curve for showers due to the photon component alone. [The actual counting rates must be corrected for a small zero effect due to lack of efficiency of the counter tray A, to chance coincidences (BCD), to showers from the side, etc. This correction was determined by placing a thick lead absorber above the counter tray A; see below.]

The experimental results obtained, at sea level, with lead as a shower-producing material are represented by the solid dots in Fig. 2. These results lend themselves to a more accurate comparison with theory than

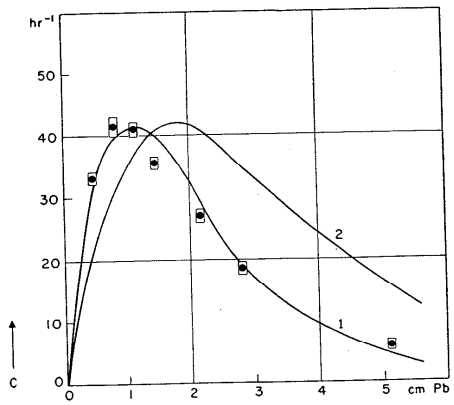

Fig. 6.8.2. The transition curve in lead for showers initiated by photons, as detected with the experimental arrangement shown in Fig. 6.8.1. The abscissa represents the thickness of the lead block, s. The ordinate represents the rate of anti-coincidences ($BCD - A$) after subtraction of a constant background, given by the anti-coincidence rate observed with 5 cm of lead in S. This background is due mainly to a slight inefficiency of tray A. To a small extent, it may be due also to secondary effects of neutrons (whose absorption in 5 cm of lead is very small). The dots are experimental points with corresponding statistical errors. The curves are theoretical transition curves computed for two different photon spectra (see text). From Janossy and Rossi (JL40.1).

do the results of the experiments described in the preceding section. In fact, in the experiment under consideration, the probability that a shower from the lead produces a coincidence (BCD) is practically equal to the probability that a particle of this shower discharges one of counters D. If the number of shower particles is small, this probability is approximately proportional to the number of particles in the shower. With a shower-producing layer of thickness t, the *average* probability of detection

for a photon of energy E_0 is then approximately proportional to $\Pi(E_0,0,t)$, the *average* number of electrons at the thickness t in a shower initiated by a photon of energy E_0. Therefore, if $\gamma(E_0)\,dE_0$ represents the number of photons with energy in dE_0 at E_0 incident upon the instrument per unit time, the counting rate, $C(t)$, recorded with a lead thickness t is given by the equation:

$$C(t) = \text{const} \int \gamma(E_0)\Pi(E_0,0,t)\,dE_0. \tag{1}$$

The above considerations cease to be valid when the photon energy, E_0, is so large (and, therefore, the corresponding shower so dense) that the probability of a discharge in counters D is no longer proportional to the number of shower particles. However, high-energy photons are rare, and a crude evaluation of their contribution to the total number of anti-coincidences is sufficient.

The curves in Fig. 2 represent counting rates computed with the method outlined above for two different assumptions concerning the incident photon spectrum, namely:

curve 1:

$$\gamma(E_0) = \frac{kE_c^2}{E_0^3} \quad \text{for } E_0 > E_c; \quad \gamma(E_0) = \frac{k}{E_0} \quad \text{for } E_0 < E_c; \tag{2}$$

curve 2:

$$\gamma(E_0) = \frac{kE_c}{E_0^2} \quad \text{for } E_0 > E_c; \quad \gamma(E_0) = \frac{k}{E_0} \quad \text{for } E_0 < E_c. \tag{3}$$

In Eqs. (2) and (3) k is a constant and $E_c = 150$ Mev (which is of the order of magnitude of the critical energy in air). The calculations were based on the values of Π computed by Arley (see § 5.4) and no account was taken of incident photons with energies smaller than 10 Mev (which is close to the critical energy in lead).

The experimental results agree quite well with the theoretical curve derived from Eqs. (2), and thus indicate that these equations represent, at least approximately, the spectrum of cosmic-ray photons in the atmosphere.

Janossy and Rossi used the experimental arrangement shown in Fig. 1 also to determine the absorption curve of the photon component of cosmic rays. To this end, they recorded anti-coincidences with a constant amount of lead between counters A and B (position s) and with lead plates of different thicknesses above counter A (position S). The results for $s = 2$ cm are given on a semilogarithmic scale in Fig. 3.

The line connecting the experimental points may be regarded as the absorption curve of cosmic-ray photons in lead, i.e., the curve representing the number of photons that traverse increasing absorber thicknesses without interaction. To justify this interpretation, consider that a photon, falling upon the screen S, may either (a) traverse the screen unaffected, or

(b) produce an electron pair or a Compton electron. In case (a) the photon has exactly the same probability of producing an anti-coincidence as if the absorber S had not been there. In case (b) a shower has already started in S; it is very unlikely that this shower may discharge counters B,C, and D without discharging any of counters A. Thus, the number of anti-coincidences observed with a given thickness of lead (after deduction of the zero effect) measures the number of photons that fail to interact in the lead.

Figure 3 shows that this number decreases with increasing lead thickness according to an approximately exponential law. This is indeed what one should expect, despite the existence of photons of different energies in cosmic rays, because, on the one hand, the absorption coefficient of high-energy photons varies slowly with energy (see Fig. 2.19.4) and, on the

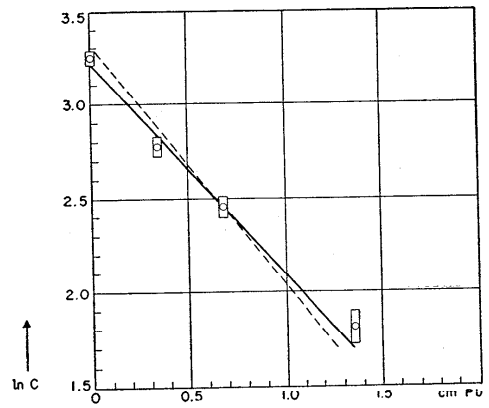

Fig. 6.8.3. The absorption curve of cosmic-ray photons in lead, obtained with the experimental arrangement shown in Fig. 6.8.1 (s = 2.0 cm Pb). The abscissa represents the thickness of the absorber S. The counting rates plotted as ordinates have been corrected for background, as explained in the caption for Fig. 6.8.2. The dashed line represents the theoretical absorption curve.

other hand, most of the observed anti-coincidences are due to photons in a fairly narrow range of energies. A least-square fit of the experimental points to an exponential curve (solid line in Fig. 3) yields a value of 0.09 ± 0.006 cm^2 g^{-1} for the absorption coefficient of cosmic-ray photons in lead. The theoretical value, computed for the spectrum represented by Eqs. (2) is 0.105. Here again, as in the experiments with artificially produced γ-rays (see § 6.2), the observed absorption coefficient in lead is slightly smaller than the theoretical one. In this case, however, the

difference is hardly significant on account of the experimental errors and the uncertainty concerning the exact shape of the photon spectrum.

V. H. Regener (RVH40), working at sea level, made a direct comparison between showers produced by photons and by ionizing particles (electrons and mesons) by means of the experimental arrangement shown in Fig. 4. In this experiment, the showers were produced in the lead block Pb and were detected by the threefold coincidences of counters A,B,C. The lead block was surrounded by ten counters marked D and was covered by nine counters marked E. The experiment consisted of recording, with various lead thicknesses, either the anti-coincidences ($ABC - DE$) or the anti-coincidences ($ABC - D$). In the first case the instrument detected shower production by photons exclusively (aside from a background correction); in the second case the instrument detected shower production by photons, electrons, and mesons. Counters D, that were connected in anti-coincidence in both phases of the experiment, served to decrease the background due to side showers.

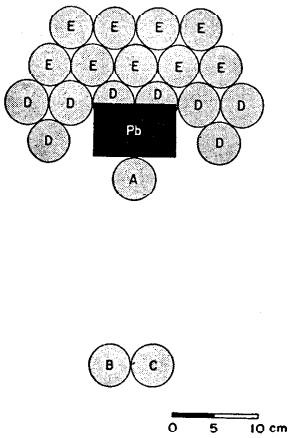

Fig. 6.8.4. Experimental arrangement used by V. H. Regener for the investigation of shower production by photons and by ionizing particles (RVH40).

The experimental results are shown in Fig. 5, where the lower curve refers to photon-produced showers and the upper curve to showers produced by photons, electrons, and mesons. The characteristic maximum occurs at about the same position for both curves. Near the maximum, the number of showers produced by photons appears to be about one-third of the total number of showers. From the height of the "tail" of the upper curve one estimates that mesons account for approximately another third of all the showers at the maximum. Thus one would conclude that high-energy electrons and photons are about equally abundant in cosmic rays. At large thicknesses the ratio between the numbers of showers produced by ionizing and by nonionizing rays, respectively, is greater than near the maximum. This is clearly due to the fact that shower production by mesons becomes increasingly important as the lead thickness increases.

In the evaluation of experiments like those described here, one must be warned against the possibility of spurious effects that may appreciably

alter their results. Thus a slight inefficiency of the anti-coincidence counters or an incomplete protection against side showers may add to the anti-coincidence rate and therefore lead to an overestimate of the number of photons; the existence of a background of this kind is probably responsible for the "tail" of the lower curve in Fig. 5. On the other hand, photons and electrons are part of showers that develop in the atmosphere.

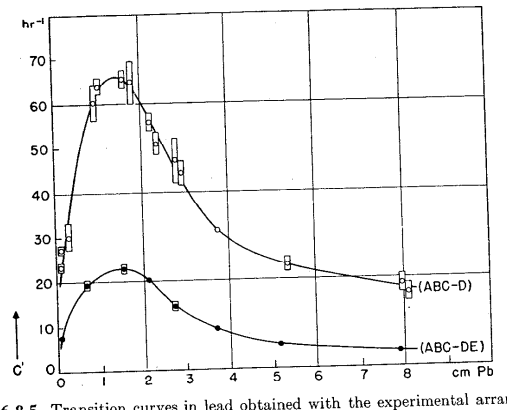

Fig. 6.8.5. Transition curves in lead obtained with the experimental arrangement shown in Fig. 6.8.4. The abscissa is the thickness of the lead block Pb. The upper curve represents the counting rate for anti-coincidences $(ABC - D)$; the lower curve represents the counting rate for anti-coincidences $(ABC - DE)$. From V. H. Regener (RVH40).

Some photons may fail to be recorded because they arrive upon the detecting equipment accompanied by electrons that discharge the anti-coincidence counters.

6.9. ***Transition effects in the absorption measurements of cosmic rays by means of integrating ionization chambers.*** In the early period of cosmic-ray research, several experimenters investigated the absorption of cosmic rays in matter by measuring the ionization current in an integrating chamber (§ 3.2) placed under increasing thicknesses of different absorbers [see, for example, the review article of Hoffmann (HG32)]. Among other results, they found that if the atomic number of the absorber is considerably greater than that of air, the ionization initially increases slightly with increasing absorber thickness, goes through a maximum and then decreases again, rapidly at first and more slowly in the successive layers. Peculiar irregularities occur also when the radiation passes from one solid absorber to another of different atomic number.

These phenomena are known as "transition effects." Figure 1, reproduced from a paper by Schindler (SH31), shows a set of typical transition curves obtained at sea level. Young and Street (YRT37) described transition curves in lead measured at various altitudes above sea level.

The following considerations explain qualitatively the transition effect observed in the passage of the radiation from air to a heavy absorber. The electrons and photons present among cosmic rays in the atmosphere have an average energy of the order of the critical energy in air; i.e., of the order of 100 Mev. This energy is many times greater than the critical

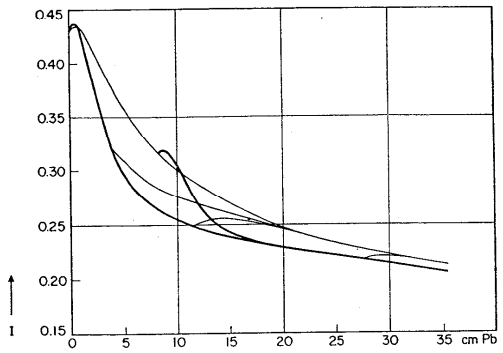

Fig. 6.9.1. A set of typical transition curves measured by Schindler (SH31) at sea level with an integrating ionization chamber. Heavy lines: lead; thin lines: iron. The ordinate represents the ionization, I, in arbitrary units. The abscissa represents "centimeters of lead equivalent." According to Schindler's definition, two thicknesses of iron and lead are called equivalent if they contain the same number of electrons per cm².

energy in heavy elements, e.g., lead. Thus as the radiation passes from air to an absorber of high atomic number, the number of electrons increases at first by cascade multiplication and goes through a maximum at a thickness of the order of the optimum thickness for showers initiated by electrons or photons of about 100-Mev energy. Beyond the maximum the number of electrons decreases rapidly and so does the total ionization recorded by the ionization chamber. After a sufficient absorber thickness, the showers initiated by the electrons and photons incident upon the absorber from the atmosphere have disappeared. The residual ionization is due entirely to mesons and to their secondary electrons. From this point on, the ionization follows the meson intensity and therefore decreases very slowly with increasing absorber thickness. Most of the secondary electrons in the absorber arise, directly or through cascade

multiplication, from knock-on processes of mesons.* In a condition of equilibrium, the total energy per g cm^{-2} spent by the mesons and by their secondary electrons in ionization or excitation of atoms equals the total collision loss of mesons (see § 2.10). This quantity is a slowly decreasing function of the atomic number, Z (see Figs. 2.9.1). Therefore, for a given meson intensity, the total ionization observed under thick layers of different absorbers should also be a slowly decreasing function of Z, even though the decrease with Z of the collision loss may be compensated partially by the increase of energy losses due to radiation and to direct pair production (see § 2.20).

Moreover, the average energy of the electrons in equilibrium with mesons is somewhat greater in substances of low Z than in substances of high Z. Thus, as the radiation passes from one absorber to another of higher atomic number, low-energy electrons are produced at a faster rate than they disappear and high-energy electrons disappear at a faster rate than they are produced; until eventually the secondary radiation acquires the energy spectrum characteristic of the second medium. Further complications arise because of the strong Z-dependence of Coulomb scattering, which is very important for low-energy electrons (see below).

Presumably, the transition effects observed at the boundary between two different absorbers depend, in part, on the change in the intensity and in the energy distribution of the electrons in equilibrium with the meson component. They are complicated by the presence of electrons and photons that are not in equilibrium with mesons, if the change of absorber occurs before the showers initiated by electrons and photons incident from the atmosphere have completely disappeared.

Before closing this section we wish to mention an interesting result obtained by Vernov and Vavilov (VSN46). These experimenters used as detectors shallow, thin-walled ionization chambers placed horizontally and took measurements with various thicknesses of lead *above* as well as *below* the chambers. They found that the presence of lead *below* the chambers increases the ionization current very considerably. They also found that the relative increase of ionization is greater with 1 cm of lead above the chamber than without any lead above the chamber. The observed increase of ionization is certainly due to back-scattering of low-energy electrons. Electrons from lead have a smaller average energy than electrons from air. Therefore they are more strongly scattered and it is thus understandable that the presence of lead above the chamber should enhance the effect of the lead below.

6.10. ***Shower experiments by means of artificially produced γ-rays.*** The development of the betatron and the synchrotron has made

* This, of course, is not true of the electrons present in the atmosphere. The main sources of these electrons are nuclear interactions of high-energy nucleons and decay processes of mesons.

available to physicists well collimated and relatively strong beams of γ-rays of known energy spectrum. With these beams one can study the cascade process in a range of energies extending to several hundred Mev more accurately than one can do with cosmic-ray electrons and photons.

Blocker, Kenney, and Panofsky (BkW50) have investigated shower production in various substances (*converters*) by the γ-radiation of the Berkeley synchrotron operated at 330 Mev. Figure 1 shows the disposi-

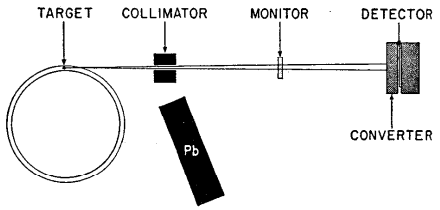

Fig. 6.10.1. Experimental arrangement used by Blocker, Kenney, and Panofsky (BkW50) to investigate shower production by 330-Mev γ-rays from the Berkeley synchrotron.

tion of the experiment. The γ-ray beam originates in a 0.05-cm-thick platinum strip placed inside the vacuum chamber that contains the circulating beam of electrons. The γ-ray beam leaves the chamber through a 2.2-cm quartz wall, and arrives upon the converter after passing through a lead collimator and a monitor chamber. The converter consists of plates of lead, copper, aluminum, or carbon placed perpendicularly to the beam. The lateral dimensions of the plates are of the order of 30 centimeters. The beam is 4.3 cm in diameter at the converter.

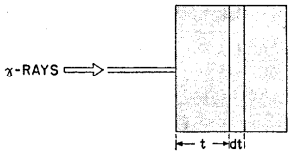

Fig. 6.10.2. Illustrating the definition of $\rho(t)\,dt$.

The equations describing the *average* behavior of showers apply directly to the cascade radiation produced in the converter by the γ-ray beam. In this respect, the interpretation of synchrotron experiments is simpler than that of cosmic-ray experiments, where one deals with showers produced by single electrons or photons and where, therefore, fluctuations from the average behavior are all important. The boundary conditions of the problem stipulate that no electrons are present at $t = 0$ [$\pi(E,0) = 0$] and that $\gamma(E,0)\,dE$ equals the number of photons with energy in dE at E incident upon the converter per unit time. With these boundary conditions, the quantity $\rho(t)\,dt$ (as defined in § 5.1) represents the ionization

loss per unit time of all shower electrons in a layer of thickness dt perpendicular to the direction of the incident beam, at a depth t from the front of the converter (see Fig. 2).

If the lateral dimensions of the layer dt are large compared with the mean lateral spread of the shower and if the material of the converter extends to a sufficient distance *beyond* the layer in question, scattering of the low-energy shower electrons has a small effect on the energy dissipation in dt (§ 5.22). If the above conditions are not fulfilled, however, the effect of scattering is very important and very difficult to compute theoretically.

In principle one can measure $\rho(t)$ by replacing an infinitely thin layer of the converter at the depth t with a layer of gas, where the energy dissipation of shower electrons gives rise to an observable ionization. In order to approach this ideal condition, Blocker and his collaborators used as a detector a shallow thin-walled, airfilled, integrating ionization chamber (sensitive volume: 27.5 cm in diameter, 1.27 cm deep) embedded in the converter as shown in Fig. 1. By removing the converter behind the chamber, they showed that back-scattering of low-energy electrons contributed very appreciably to the measured ionization current. This is in agreement with the qualitative predictions of the theory and with the experimental results mentioned in §§ 6.6 and 6.9. At the shower maximum, the ionization due to back-scattering was 41 per cent of the total for lead, 20 per cent for copper, 9 per cent for aluminum, and 4 per cent for carbon. The critical dependence of back-scattering on atomic number of the converter shown by the above figures is also in agreement with the theory.

The finite width of the slot where the ionization chamber lies appreciably modifies the measured ionization current because it allows some of the widely scattered electrons to escape laterally without dissipating all of their energy in the chamber. To correct for this effect, Blocker and his collaborators took measurements with slots of several widths, from 3.8 to 1.9 cm, and extrapolated the ionization values to zero slot width. The correction is a decreasing function of atomic number and depends on the thickness of the converter in front of the chamber, as one might have expected. For lead and for a slot width of 1.9 cm the correction is of the order of 20 per cent near the maximum of the shower curve. For aluminum and carbon the correction is negligible.

Figure 3 shows the results obtained with the various substances investigated. In this figure the abscissa represents the thickness of the converter in g cm^{-2}. The ordinate represents, on a logarithmic scale, the ratio of the ionization current in the detector chamber to the ionization current in the monitor chamber, extrapolated to zero slot thickness as explained above. Thus the various experimental curves effectively correspond to the same beam intensity.

In all substances, the total absorption coefficient of γ-rays goes through a minimum at a certain value of the γ-ray energy (see Figs. 2.19.3 and

2.19.4). One may predict that, with increasing converter thicknesses, the shower curve in any given substance tends to become exponential, with a logarithmic slope corresponding to this minimum absorption coefficient (§ 5.15). Within the errors of the measurements, the experimental results confirm this prediction (see Fig. 3).

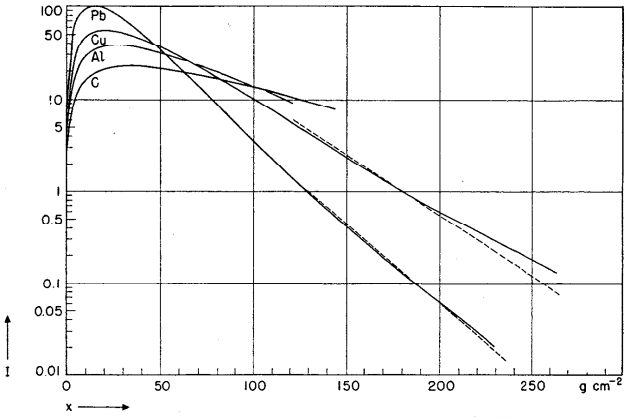

Fig. 6.10.3. Experimental results obtained with the arrangement shown in Fig. 6.10.1. The total ionization, I, in a converter of effectively infinite lateral dimensions plotted against the depth, x, in the converter; x is in g cm^{-2}, I in arbitrary units. The dashed lines have slopes calculated from the minimum absorption coefficients of γ-rays. The discrepancies between the slopes of these lines and of the experimental curves are considered to be within the experimental errors. From Blocker *et al.* (BkW50).

From the ionization current measured with the chamber behind a thickness t of the converter one can compute the energy dissipation in the converter at the depth t, $\rho(t)$. To see this, consider that the ionization current (in number of ion pairs per second) multiplied by the energy per ion pair, V_0 (§ 2.10), and divided by the depth of the chamber in radiation lengths gives the energy dissipation of all shower electrons per radiation length of the gas and per second. Because of the small thickness of the chamber walls (0.0067 cm aluminum) there is no appreciable change in the composition of the shower radiation as it passes from the converter into the chamber. Moreover, the energy dependence of the ionization loss of electrons is approximately the same in all substances. Therefore the energy dissipation per radiation length in the converter is closely proportional to the energy dissipation per radiation length in the gas. The proportionality constant is the ratio of the ionization losses of electrons per radiation length of the two materials.

The area under the curve representing $\rho(t)$ (or the area under the curve representing the energy dissipation per g cm^{-2} as a function of thickness in g cm^{-2}) equals the energy per unit time of the incident beam. Table 1 lists the values of the incident energy that one obtains from the experimental curves in Fig. 3, extrapolated to infinite thickness with exponential curves corresponding to the minimum absorption coefficient of γ-rays. These energy values should all be the same because, as pointed out above, the various curves effectively correspond to the same beam intensity. The experimental figures differ by as much as 16 per cent. This discrepancy is a measure for the errors involved in the various approximations made in the evaluation of the experimental results.

Table 6.10.1. Areas below the curves in Fig. 6.10.3

Converter:	C	Al	Cu	Pb
Area:	100.4	103.0	94.6	84.6

6.11. ***Cloud-chamber pictures of cosmic-ray showers.*** Cloud-chamber observations of cosmic-ray phenomena have yielded striking examples of electronic showers. Pictures obtained with multiple-plate cloud chambers [first used for this purpose by Street (SJC39)] are particularly interesting as they illustrate most clearly the cascade process leading to the development of these showers. One of these pictures, representing a shower initiated by a photon, has been reproduced in Fig. 5.1.1. In this picture one will notice the following features.

(a) The number of electrons in the shower increases at first with increasing thickness of matter traversed and then decreases again, as predicted by the theory. The maximum seems to occur below the fourth plate, i.e., after approximately 8.6 radiation lengths. This corresponds to a primary energy of approximately $7 \cdot 10^9$ ev (see Fig. 5.22.1), for which the number of particles at the maximum is about 70 (see Fig. 5.22.2). The cloud-chamber picture is not sufficiently distinct to allow individual electron tracks to be counted at the maximum; the appearance of the picture, however, is not inconsistent with the above estimate.

(b) The shower has a dense and narrow core that gradually disappears. This core contains the high-energy electrons and photons responsible for the further propagation of the shower. Particles coming out of a lead plate at wide angles are low-energy electrons. They usually come to rest in the next lead plate, without producing secondaries. Thus, at least in the early stages of the development, the shower particles appearing under each plate seem to come approximately from a point located in this plate, and, if the rest of the picture is ignored, give the false impression of being produced in a single act. The disappearance of the core shows that the shower is "growing old," i.e., that it no longer contains high energy particles capable of further multiplication and will soon die. Toward the tail end, low-energy photons, which are produced in great abundance and with large angular spread during the development of the shower, become very important, as evidenced by the large number of slow-electron tracks appearing in the lower sections of the chamber.

(c) If we imagine that the gaps between the plates are reduced to zero, we obtain a picture for the propagation of a shower in solid material. The shower diverges at first but then maintains approximately constant lateral dimensions until it approaches the end. This is due to the strong absorption of the low-energy electrons scattered out of the core. The radius of the cylinder that contains most shower particles is of the order of magnitude of the range of these particles, which, in turn, is of the order of one radiation length. The electrons appearing outside of this cylinder are produced mainly by low-energy photons. Compared with the more energetic components of the shower, they become progressively more important as the shower approaches its end.

(d) The shower picture reproduced in Fig. 5.1.1, as well as many other similar pictures found in the literature, fail to show any evidence of nuclear interactions. This proves that nuclear interactions are not an important effect in the development of showers initiated by electrons or photons.

Figure 1 is the picture of a shower obtained by Butler and his collaborators (BCC50) with a cloud chamber operated under 10 cm of lead. The chamber contains a 3-cm-thick lead plate and is placed in a magnetic field of 6,400 gauss. Above the plate one sees a number of positive and negative electrons of comparatively low energy. One also sees a dense and narrow core of very energetic electrons. This core undergoes tremendous multiplication on traversing the lead plate. According to a crude estimate there are about 500 electrons below the plate. They have mostly fairly low energies. The energy of the primary particle that has produced this shower cannot be much smaller than 10^{11} ev. Unlike most shower pictures, Fig. 1 shows evidence for a nuclear interaction originating from the core of the shower.

Nassar and Hazen (NS46) made an attempt to check the shower theory quantitatively using pictures obtained by means of a cloud chamber equipped with 4 lead plates, each 0.7 cm thick, and operated in a magnetic field of 1,100 gauss. This field was sufficient for measuring momenta up to about $25 \cdot 10^6$ ev/c. The expansions were controlled by a counter telescope placed above the chamber.

Among 1,500 photographs, there were 53 with cascade showers initiated by electrons. From this group the authors selected 11 showers with approximately the same total number of electron tracks, namely 8 to 11 (this includes tracks appearing under all four plates). Next they computed an "average" shower curve by plotting the average number of particles under each lead plate against the total thickness of lead above. This they did both considering all electron tracks, irrespective of momenta, and selecting electron tracks with momenta greater than $3.5 \cdot 10^6$ ev/c.

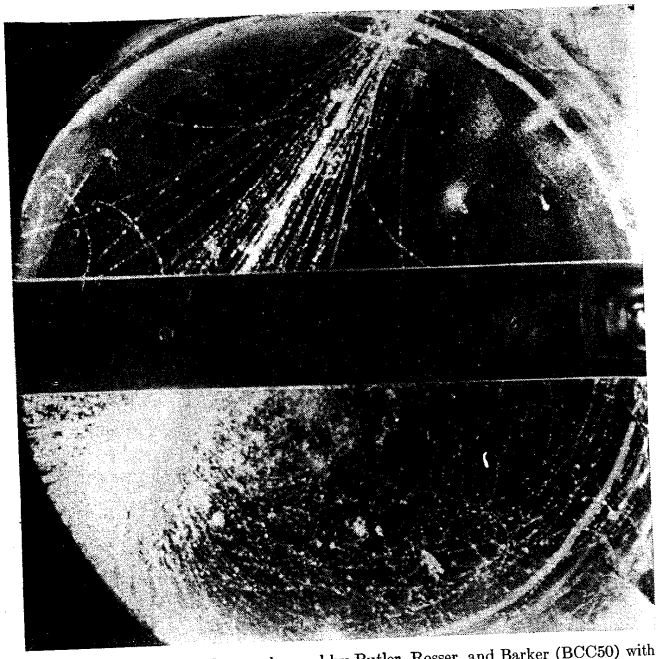

Fig. 6.11.1. A large shower observed by Butler, Rosser, and Barker (BCC50) with a cloud chamber operated in a 6,400-gauss magnetic field. The shower is initiated in a lead block above the chamber by an electron or photon of very great energy. It undergoes strong multiplication in the plate across the chamber (3 cm of lead with 0.18 cm of brass on each side). The event is unusual in that a nuclear "star" appears to originate from the core of the shower.

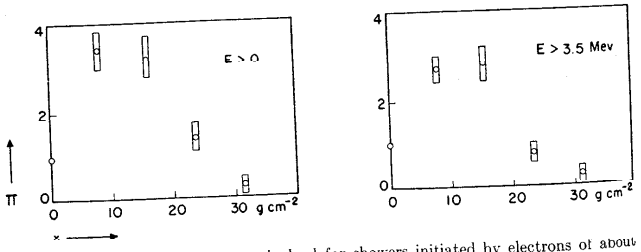

Fig. 6.11.2. Transition curves in lead for showers initiated by electrons of about 230-Mev energy. Abscissa: thickness, x, in g cm^{-2}; ordinate: average number of electrons, $\Pi(E)$, of all energies ($E > 0$) and of energy greater than 3.5 Mev ($E > 3.5$ Mev). From the cloud-chamber experiments of Nassar and Hazen (NS46).

Figure 2 shows the results. Presumably the eleven showers selected were initiated by electrons of approximately the same energy. The authors determined this energy experimentally by computing the total energy loss in lead for the average shower. This quantity (see §§ 5.13 and 5.18) is given by the critical energy times the area under the curve representing the total number of electrons as a function of thickness in radiation lengths. The energy thus obtained was 230 Mev. According to Fig. 5.22.2, the corresponding value of Π_{max} is about 2.7; the experimental curve in Fig. 2 gives for Π_{max} a value of 3.5 ± 0.5.

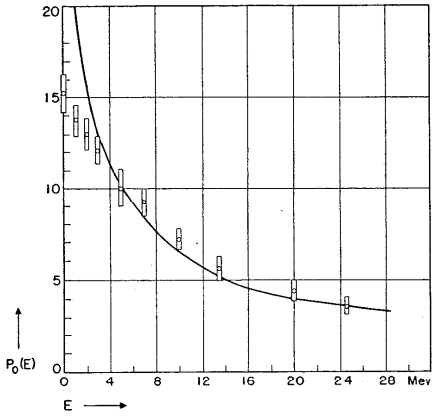

Fig. 6.11.3. The observed number of electrons with energy greater than E at the shower maximum in lead compared with the integral track length distribution, $P_0(E)$, given by the formula of Tamm and Belenky. The absolute values of P_0 are arbitrarily normalized to fit the experimental data at about 5 Mev. From the cloud-chamber experiments of Nassar and Hazen (NS46).

Nassar and Hazen also determined the average energy distribution of electrons near the maximum, making use of 17 showers with a maximum number of particles between 6 and 20. To consider showers of different sizes for the purpose of this determination is not objectionable because, according to theory, the energy distribution of shower electrons near the maximum does not depend markedly on the primary energy, if this is large compared with the energy of the electrons under consideration.

Theoretically, the function representing the integral energy spectrum near the maximum is closely similar to that representing the integral track length (see § 5.10). In Fig. 3 the points show the experimental results of Nassar and Hazen and the curve represents the integral track length, as given by the formula of Tamm and Belenky, under the assumption that

the energy of the initiating particle is large compared with the critical energy. For shower electrons of energy greater than about 3 Mev the agreement is quite satisfactory, discrepancies at lower energies may be explained by deficiency of the theory, due, mainly, to the neglect of scattering.

The reader will find in ref. (CKM50) the description of a cloud-chamber experiment on showers produced by γ-rays from a 320-Mev synchrotron.

6.12. ***Cloud-chamber evidence for electromagnetic interactions of mesons.*** Cloud-chamber pictures occasionally show examples of secondary events that can be best explained as electromagnetic interactions (collision processes, radiation processes, or pair production) of cosmic-ray particles heavier than electrons. These particles could be mesons or protons. However, both at sea level and at mountain altitudes, mesons (or more specifically, μ-mesons) are present in much greater numbers than protons. Moreover, for a given energy, μ-mesons have a somewhat greater probability than protons for collision processes (see § 2.3) and a much greater probability for radiation processes or pair production (see §§ 2.14 and 2.20). One is thus justified in classifying as a μ-meson any cosmic-ray particle heavier than an electron that is observed to undergo an electromagnetic interaction.

Figure 1 shows an electromagnetic interaction. The event taking place is, most likely, the production of a secondary electron by a collision process of a μ-meson.

Various investigators have obtained statistical information on the average number of secondary electrons in equilibrium with mesons in heavy materials. Hazen, for example (HWE43.3), observed an average number of 0.07 secondary electrons per meson emerging from a lead plate of 0.7-cm thickness. Brown, McKay, and Palmatier (BWW49) found about the same relative number of secondary electrons in a series of pictures obtained with a cloud chamber containing five 1.27-cm-thick lead plates. These authors also measured the distribution of the projected angle between the trajectory of the meson and that of the secondary electron emerging from the lead, which is shown by the histogram in Fig. 2. Since the plates were horizontal and the chamber was controlled by a telescope selecting nearly vertical mesons, the observed distribution practically coincides with the distribution, relative to the direction normal to the plates, of secondary electrons arising from mesons incident perpendicularly upon the plates. It is important to note that this distribution does not even approximate the angular distribution of the secondary electrons at their place of production, but is determined mainly by the scattering properties of the plates.

That scattering plays an important role in the phenomena considered here is proved most clearly by the comparatively large number of "back-scattered" electrons, i.e., of electrons that emerge from the surface through which the mesons enter the plate. This number, according to Brown and

his collaborators, is about 0.02 per meson, to be compared with a number of 0.07 electrons per meson emerging from the surface through which the mesons leave the plate.

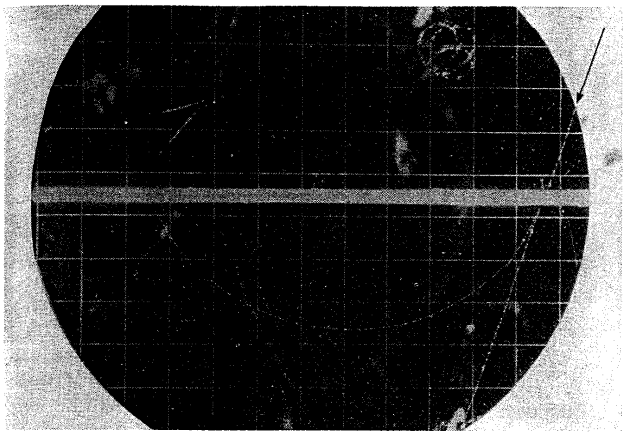

Fig. 6.12.1. Production of a secondary electron of about 5 Mev energy in the passage of a μ-meson through a 0.63 cm thick aluminum plate (R. W. Thompson).

The observations of these authors show also that about 87 per cent of all secondary electrons appear single and the remaining 13 per cent in very small groups. Most of the secondary electrons that accompany mesons in their passage through matter arise from collision processes. In qualitative agreement with the theoretical predictions, the above result indicates that these processes usually produce electrons of moderate energies, which do not give rise to large showers.

6.13. ***Production of ionization bursts by showers.*** Electronic showers traversing an ionization chamber produce bursts of ionization whose size is related to the number of shower particles. Thus the observation of ionization bursts offers another method for the detection of showers. Several investigators have used this method to study shower production in various thicknesses of matter. Among other results, they have obtained shower curves similar to those observed with Geiger-Mueller counters (see § 6.7).

However, as we shall discuss later in more detail (§ 8.3), electronic showers are not the only, and often not even the most important cause of

ionization bursts. For this reason, and for the sake of brevity, we do not intend to undertake here a discussion of burst experiments except for mentioning one of their most important results.

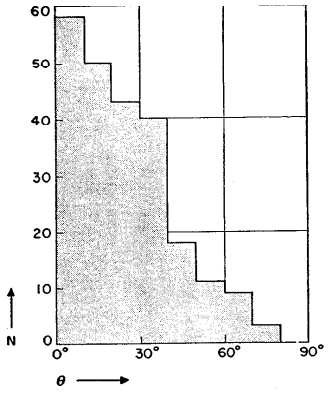

Fig. 6.12.2. Angular distribution of knock-on electrons produced in 1.27 cm thick lead plates by μ-mesons of energy greater than 200 Mev. The abscissa, θ, represents the angle between the trajectory of the primary meson and that of the secondary electron, projected on the plane of the cloud chamber. The ordinate, N, represents the number of particles per 10^0 interval. From Brown, McKay and Palmatier (BWW49).

Schein and Gill (SM39), working at sea level, measured the rate of occurrence of bursts of different sizes in a spherical ionization chamber with 1.25-cm-thick steel walls, surrounded by 10.7 cm of lead. The circles in Fig. 1 represent their experimental results.

Christy and Kusaka (CRF41.2) compared the observed burst rates with those computed under the assumption that all bursts recorded in the experiment of Schein and Gill are due to showers arising from knock-on and radiation processes of mesons. They made this computation for mesons of spin 0, $\frac{1}{2}$, and 1. By taking into account the known energy spectrum of cosmic-ray mesons, they obtained the curves shown in Fig. 1.

The theoretical results are subject to considerable uncertainty, for several reasons. Christy and Kusaka assumed that the high-energy μ-mesons falling upon the instrument were distributed isotropically in direction (which is almost certainly incorrect) and neglected fluctuations in the computation of the distribution of shower sizes. One may add that the method used to correlate pulse heights with shower sizes also is questionable. Particularly difficult to compute is the transition effect that occurs in the passage of the shower radiation from the lead absorber to the iron of the chamber walls. However, despite the possibility of a large error in the computed burst curves, a comparison between these and the experimental data clearly favors spin 0 or $\frac{1}{2}$. Mesons of spin greater than $\frac{1}{2}$ should definitely produce many more large bursts than actually are observed.

We have mentioned repeatedly that practically all of the mesons in the atmosphere are μ-mesons. From their mode of decay we know that μ-mesons have half-integer spin. From the burst data we can now rule

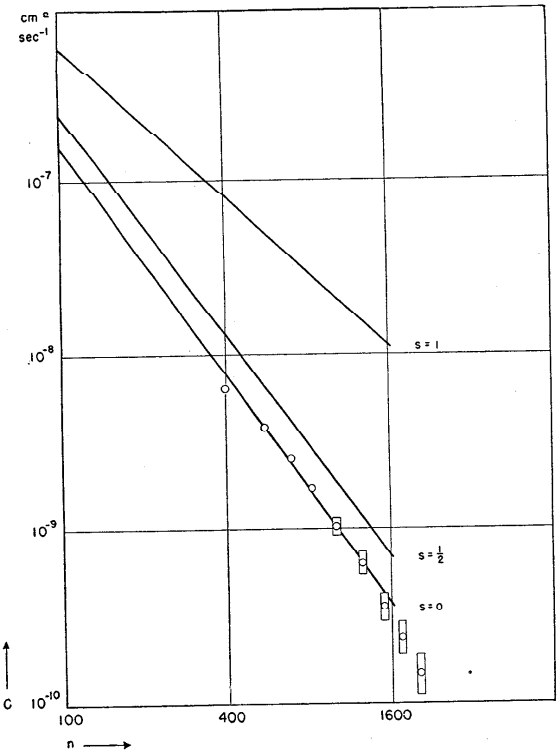

Fig. 6.13.1. The integral pulse-height distribution for bursts observed at sea level in a spherical ionization chamber surrounded by lead. The abscissa is the number of minimum ionizing particles which, on traversing the chamber, produce a burst of the observed size. The ordinate is the number of bursts of size greater than the corresponding abscissa (per second and per cm² of the chamber projected area). The circles represent experimental points obtained by Schein and Gill. The curves represent the burst rates due to collision and radiation process of mesons of spin 0, $\frac{1}{2}$, and 1 respectively, as computed by Christy and Kusaka (CRF41.2).

out the possibility of spin $\frac{3}{2}$ or greater and we thus conclude that the spin of μ mesons is $\frac{1}{2}$.

Notice that the above conclusion has even greater strength if one considers that some of the bursts recorded by Schein and Gill are almost certainly due to phenomena different from electromagnetic interactions of μ-mesons (e.g., nuclear interactions of protons and air showers).